ADVANCED MATERIALS
www.advmat.de

Touch- and Brush-Spinning of Nanofibers

*Alexander Tokarev, Darya Asheghali, Ian M. Griffiths, Oleksandr Trotsenko, Alexey Gruzd, Xin Lin, Howard A. Stone, and Sergiy Minko**

Polymer nanofibers are used in numerous applications ranging from the design of new composite materials to the fabrication of nanostructured biomimetic scaffolds for artificial bones and organs for regenerative medicine. Here, we describe a simple controllable setup for drawing single filament nanofibers from polymer solutions or melts using a rotating rod or a set of rods (round brush). The setup can be assembled in a few minutes and applied to fabricate customized nanofiber scaffolds and meshes for various applications. The resulting fiber diameter is controlled precisely in the range 40 nm to 5 μm by adjusting the rotational speed and polymer concentration. Owing to the simple design and capability to manipulate single nanofibers, the spinning setup can be used to wind a single filament into unidirectional, orthogonal, or randomly oriented 2D and 3D meshes with controlled density, thickness, and combinations of different fibers and materials in the scaffolds. The method is scalable and can be implemented easily for laboratory and industrial manufacturing.

In the past decade polymer nanofibers have found applications in many different areas such as bone and tissue regeneration,[1] biosensors,[2] fuel cells,[3] design of composites,[4] and polymer nanofiber films.[5] Water/air purification systems, personal care products, and membranes utilize the high surface area of nanofibers to enhance transport and filtration properties,[6] while nanofibers with tunable conductivity and structural memory are promising building blocks for miniaturized devices.[7] Currently, electrospinning is the most popular method for nanofiber production.[8] In this method, a droplet of polymer solution is stretched to form a fiber by a high-voltage electric field. Electrospinning requires high voltages (20–30 kV) and depends strongly on the dielectric properties of materials[8a] that call for adjustment of spinning solutions and experienced operators of the spinning setup. Fibers are deposited on collectors (plane electrodes or frames) or rotating electrodes of a cylindrical shape for the fabrication of 2D and 3D fibrous nonwoven structures.[9]

Dr. A. Tokarev, D. Asheghali, O. Trotsenko, A. Gruzd, Dr. X. Lin, Prof. S. Minko
Nanostructured Materials Laboratory
The University of Georgia
Athens, GA 30602, USA
E-mail: sminko@uga.edu
Dr. I. M. Griffiths
Mathematical Institute
University of Oxford
Oxford OX2 6GG, UK
Prof. H. A. Stone
Department of Mechanical and Aerospace Engineering
Princeton University
Princeton, NJ 08544, USA

DOI: 10.1002/adma.201502768

The recent discovery of the ability of nanofibers to help to form bones and tissues in combination with stem cells[10] has resulted in a significantly increased interest in the development of simple methods for nanofiber fabrication that can be conducted in biological and biomedical laboratories. However, problems of antigenicity and immunogenicity of a donor's biological materials, as well as specific needs in the shapes, dimensions, and morphologies of tissue implants call for the fabrication of customized scaffolds[11] that can be engineered and fabricated at a health-provider facility.

The simplest method of nanofiber fabrication is direct drawing from a polymer solution using a glass micropipette.[12] This method, however, was not scaled up and thus did not find practical applications.[13] Here, we introduce a scalable method of nanofiber spinning named touch-spinning. A glass rod (0.3 mm to a few mm in diameter) is glued to a rotating stage, whose diameter can be chosen over a wide range of a few centimeters to more than one meter (**Figure 1**a). A polymer solution is supplied, for example, from a needle of a syringe pump that faces the glass rod. The distance between the droplet of polymer solution and the tip of the glass rod is adjusted so that the glass rod contacts the polymer droplet as it rotates (Figure 1b). Following the initial "touch," the polymer droplet forms a liquid bridge. As the stage rotates, the bridge stretches and fiber length increases, with the diameter decreasing due to mass conservation (Figure 1c). The surface area of the liquid thread increases with its elongation and thus generates a larger surface area for eventual solvent evaporation from the thread. For a polymer melt, the fiber drawing is followed by cooling of the polymer.

The touch-spinning setup was used for drawing polyethylene oxide (PEO) fibers from aqueous solutions. However, after several revolutions, a large amount of dried polymer accumulated on the surface of the glass rod due to wetting of the rod by the PEO solutions and its subsequent spreading; as the PEO droplets solidify on the glass rod, fiber drawing becomes impossible. In order to avoid this problem, we coated the rod with 1H,1H,2H,2H-perfluorodecyltriethoxysilane (PFSTEOS). For the fluorosilane surface-modified rod, the advancing contact angle was measured to be $\Theta_a = 118°$ for water and $\Theta_a = 107°$ for a 3.5 wt% PEO solution, while the receding contact angles were $\Theta_r = 98°$ and $\Theta_r = 75°$, respectively, indicating wetting hysteresis (Figures S1 and S2, Supporting Information). Even though the modified glass rod repelled water, the setup produced nanofibers because the modified surface adhered to the polymer solution droplet due to the wetting hysteresis. The modification with PFSTEOS aids in avoiding accumulation of the polymer on the glass rod surfaces due to nonwetting or partial wetting, thus providing conditions for excellent reproducibility of fiber drawing due to the self-cleaning properties of the rod. The same results were obtained for superoleophobic coatings of the rod surface that provides coating morphology

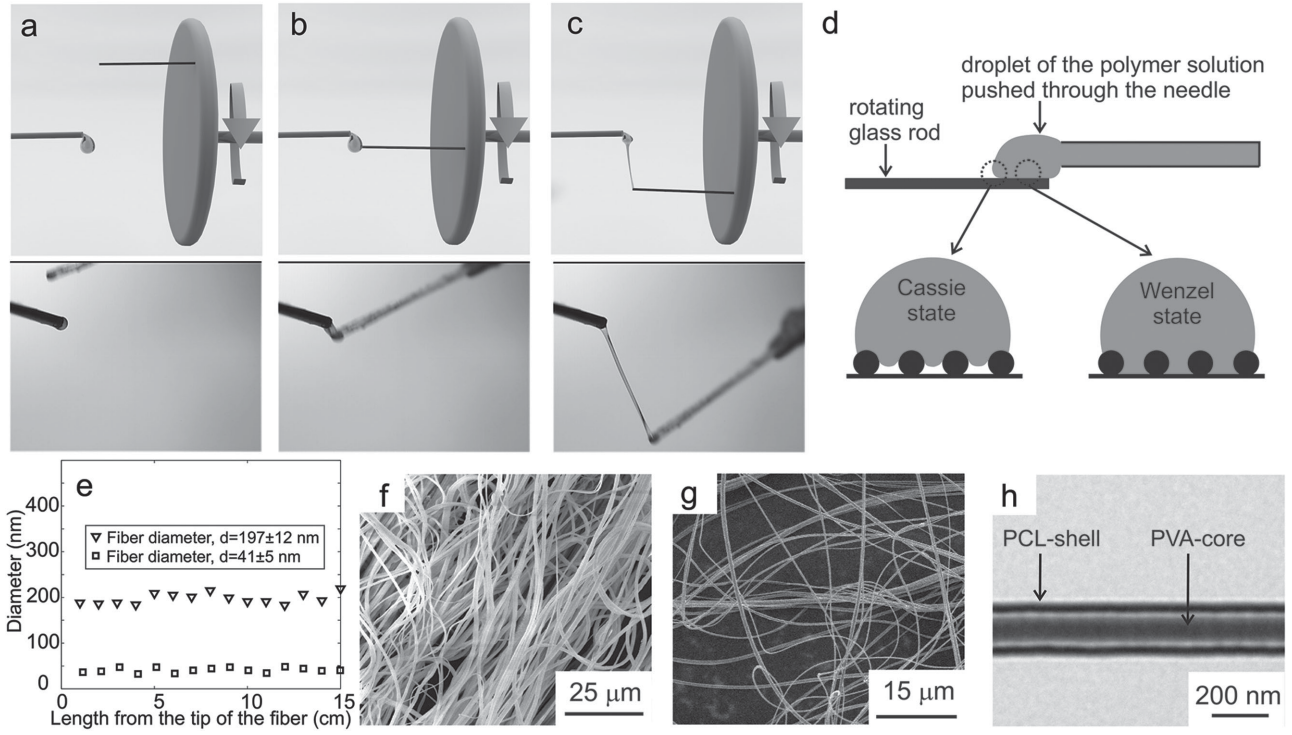

Figure 1. Touch-spinning of nanofibers. a) A glass rod is glued to a rotating stage and a droplet of the polymer solution is pushed through the needle with an automated pump. b) The rotating glass rod touches the droplet of the polymer solution. c) The glass rod continues rotation, and a liquid bridge is formed between the glass rod and the needle tip. The liquid bridge solidifies upon solvent evaporation (or cooling for polymer melts) and fibers are collected along the edge of the rotating stage on mounted bars (not shown here). d) The rotating glass rod touches the polymer solution droplet at a high speed and thus the local pressure overcomes the breakthrough pressure, resulting in wetting hysteresis due to the transition to the Wenzel complete-wetting state while further spreading of liquid outside the high pressure area is limited by partial wetting or nonwetting Cassie states. e) The fiber diameter along a 15 cm length of a PEO (triangles) and PCL (squares) fiber. f) scanning electron microscope (SEM) image of PEO nanofibers. g) SEM image of Teflon nanofibers. h) transmission electron microscope (TEM) image of a core–shell polyvinyl alcohol (PVA)–PCL nanofiber.

of re-entrant geometry (Figure S3, Supporting Information). The local pressure (≈10^6 Pa) generated when the rotating rod hits the droplet is much greater than the breakthrough pressure for typical composite surfaces with a re-entrant geometry (≈10^3 Pa).[14] This results in a transition from Cassie to the fully wetted Wenzel state (Figure 1d), causing wetting hysteresis. For polymer solutions in aqueous and organic solvents, all of the coatings were found to have no buildup of polymer layers on the surface of the rod. Our results demonstrate that the touch-spinning method can be realized when the wetting behavior of the rod is optimized to nonwetting or partial wetting with wetting hysteresis.

Examples of touch-spun PEO nanofibers are shown in the scanning electron microscopy (SEM) image in Figure 1f. The resulting fibers are very close to homogeneous in diameter along the fiber length (Figure 1e). This method is not sensitive to the dielectric properties of the polymer solutions and thus can be used to draw a range of fibers from various polymer solutions and melts. For example, Teflon nanofibers can be fabricated by electrospinning only if blended with another polymer,[15] since Teflon is only soluble in liquids with low dielectric constants. Here we used the touch-spinning method to produce Teflon nanofibers from a solution of TAF 1600 (copolymer of 2,2-bis(trifluoromethyl)-4,5-difluoro-1,3-dioxole) in Fluorinert FC-40 fluid with dielectric constant 1.9 (Figure 1g). The touch-spinning method can also be used for drawing fibers from polymer melts. For example, touch-spun polyethylene microfibers were drawn from polyethylene (PE) melted by a heat gun at 150 °C (Figure S4, Supporting Information). Moreover, we used the touch-spinning method to produce core-shell poly(vinyl alcohol) (PVA)-polycaprolactone (PCL) nanofibers (Figure 1h) using a needle with a coaxial needle.

In the touch-spinning method, the resulting nanofiber diameter can be varied by changing the rotation speed of the stage or the concentration of the polymer solution. **Figure 2**a summarizes variations in fiber diameter as a function of PEO concentration in the range from 3.5–9 wt% and as a function of rotational speed in the range 500–2500 rpm: the fiber diameter decreases with increasing rotational speed and decreasing polymer concentration. Standard deviations of the fiber diameter in a series of experiments are presented in Table S3 (Supporting Information), and are comparable with those for fibers made using other traditional nanofiber spinning methods.[16] In each series, the standard deviation was measured for one hundred 15 cm-long fibers in different samples of the same batch along the fiber's length. For example, the standard deviation for 125 nm fibers is ±36 nm, while for each given filament along its contour, the variation of diameter is much smaller (±10 nm).

Adv. Mater. **2015**,
DOI: 10.1002/adma.201502768

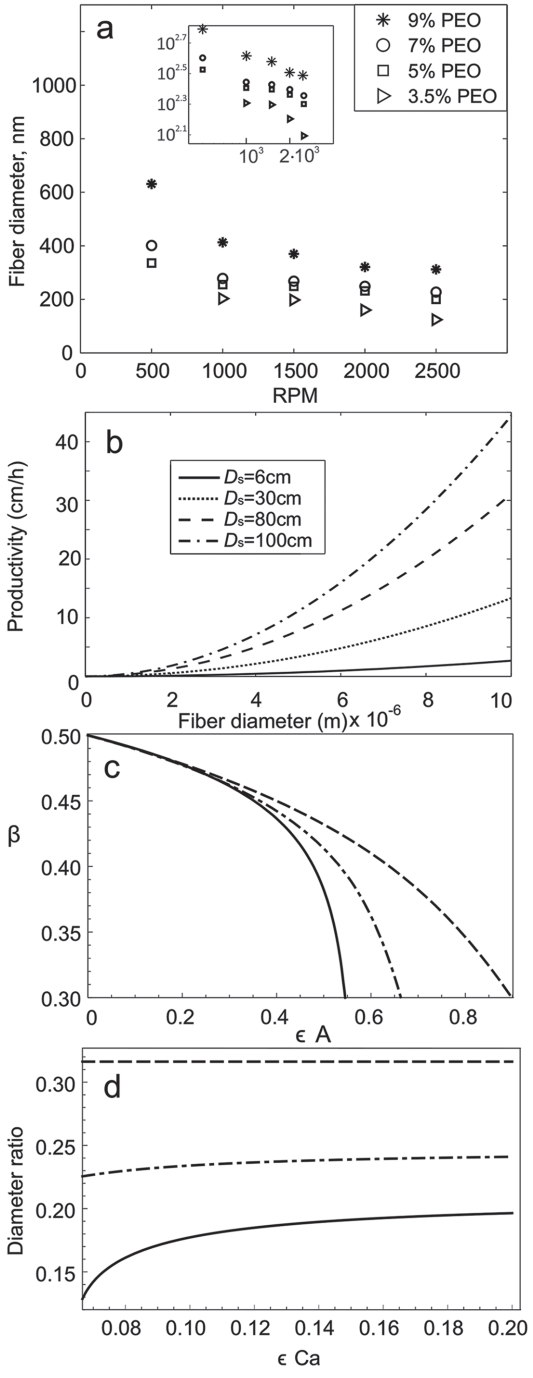

Figure 2. Controlling the diameter of fibers produced by touch-spinning. a) Diameters of touch-spun PEO nanofibers at different rotational speeds. Standard deviations of the fiber diameter in a series of experiments are presented in Table S3 (Supporting Information). Inset shows graph A with log–log axes, demonstrating a simple power law. b) Productivity of touch-spinning, where D is the diameter of the rotating stage. c) Plot of exponent β versus evaporation parameter, ϵ A for the illustrative example of ϵ Ca = 1 (dashed line), 10 (dashed–dotted line), and 20 (solid line) for a fiber draw ratio of 10. We observe a decrease in the power with increasing evaporation rate and with increasing surface tension. d) Ratio of the final fiber diameter to diameter of the fiber as it emerges from the droplet versus ϵ Ca. As ϵ Ca increases (i.e., as viscosity decreases), the final fiber diameter decreases. Here ϵ A = 0 (dashed line), 0.4 (dashed–dotted line), and 0.6 (solid line).

A series of experiments with different diameters of glass rods (from 0.33 to 1.8 mm) and different wetting properties of the surface of the rods (water contact angle from 0° to 160°) demonstrated no effect on the fiber diameter, which indicates that the fiber diameter is a function of the interplay of parameters for stretching of the polymer liquid formed between the surface supplying the polymer liquid and the tip of the glass rod, as discussed below. The wetting behavior of the rotating rod is critical to avoid contamination of the rod with polymer deposits. The wetting behavior and diameter of the rod have no effect on the fiber diameter (Table S1 and S2, Supporting Information). The volumetric rate of production of fibers in touch-spinning (V_p) clearly depends on the diameter of the rotating stage (D_s), angular velocity (ω), and fiber radius (R_f) such that $V_p = \pi R_f^2(\pi D_s \omega)$. The productivity of the method estimated for a single rod is in the same range as for electrospinning[16a] (Figure 2b). The efficient range of rotation speed is 500–2500 rpm that varies with polymer structure and concentration. At speeds below 500 rpm, fibers were nonuniform with formation of beads. Supply of the polymer solution is adjusted to avoid dripping so that all the supplied liquid is picked up by the rotating rod in the steady-state regime. No effect of the needle diameter or solution droplet at the needle tip on the fiber diameter was observed.

During drawing, the fiber thins via two distinct mechanisms: axial stretching due to the rotation of the stage, and capillarity, which acts to drain fluid from the fiber back into the source droplet. When operating in steady state, the fabrication process sufficiently far from breakup may be described by exploiting the slenderness of the fiber[17] to write simplified 1D governing equations for a mass balance, including solvent evaporation and an axial linear momentum balance:

$$\frac{\mathrm{d}}{\mathrm{d}z}(R^2 w) = -\alpha R \tag{1}$$

$$\frac{\mathrm{d}}{\mathrm{d}z}\left(3\mu R^2 \frac{\mathrm{d}w}{\mathrm{d}z}\right) + \gamma \frac{\mathrm{d}R}{\mathrm{d}z} = 0 \tag{2}$$

Here, R is the fiber radius and is the fluid velocity, both of which vary with z, the axial position along the fiber; γ and μ are the fluid surface tension and viscosity, respectively; and α is a coefficient that characterizes the evaporation rate (m s^{-1}). The viscosity μ will in principle depend on the extension rate due to the presence of the polymer and the changes in the polymer concentration (which will increase as the solvent evaporates). In the region near where the fiber is drawn from the droplet, the axial stresses supported by the polymers will balance the increasing capillary pressure. This results in a viscosity that increases at a rate that is inversely proportional to the radius of the fiber emerging from the droplet.[18] However, within the main fiber, the polymers are expected to reach their maximum extension and so the viscosity attains a constant value.[18] The viscosity will also vary with time due to the solvent evaporation, but we expect that the majority of the evaporation will occur following fiber drawing, over a longer timescale (seconds). Based on these observations, we assume a constant viscosity in the model (1)–(2). We emphasize that the results we present here

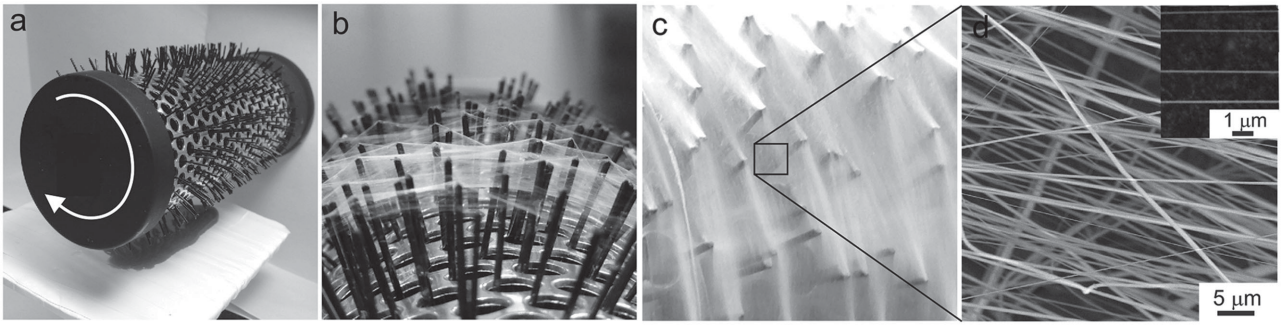

Figure 3. Brush-spinning of nanofibers. a) A round hairbrush is attached to a rotating motor and the PEO solution is poured onto a Teflon substrate. PEO solution is mixed with a dye for visualization purposes. b) Nanofibers collected on the hairbrush rotated at 3000 rpm for 1 min and c) for 5 min of spinning. d) SEM image of brush-spun nanofibers.

readily generalize for more complex viscosity relations that may be inserted directly into this model system, but we will show that this model contains the essential physics required to explain the experimentally observed phenomena.

Non-dimensionalization of Equation (1) and (2) indicates that the system may be characterized by three dimensionless parameters: the ratio of initial fiber radius as it emerges from the droplet to the length of the fiber, from the droplet to the stage, ϵ; the capillary number, $\mathrm{Ca} = \mu W/\gamma$, where W is the typical speed of withdrawal of fluid from the droplet; and $A = \alpha/W$, which measures the evaporation speed compared with the typical axial velocity.

The diameter of the fibers fabricated by the touch-spinning process may be tailored in a variety of simple ways as we have shown, for example, by adjusting the speed of the rotating stage or the polymer concentration (Figure 2a). The empirically observed fiber diameter D obeys an approximate power-law relation $D \sim \omega^{-\beta}$, where $\beta < 1/2$ (Figure 2a). Solving Equation (1) and (2) provides the relationship between β and evaporation and surface tension. The exponent β is reduced with increasing evaporation (with $\beta = 1/2$ in the absence of evaporation) and with increasing surface tension (Figure 2c). We note that we require both evaporation and surface tension to achieve a power law that differs from $\beta = 1/2$, regardless of the functional form of the viscosity.

A key advantage of the touch-spinning process is its ability to generate fibers with a uniform diameter (Figure 1e). In the touch-spinning operating regimes the reduced capillary number, $\epsilon\mathrm{Ca} \ll 1$. In this limit, Equation (2) reduces to $\mathrm{d}R/\mathrm{d}z = 0$ and so $R = R(t)$ only. This indicates that the surface tension will act to smooth out any axial variations in radius during the drawing stage (which typically occurs on a millisecond timescale) and hence we expect to observe uniform thinning for the bulk of the fiber, with variations in the fiber radius constrained to a small boundary layer of order $\epsilon\mathrm{Ca}$ times the fiber length near where the fiber emerges from the droplet. Within this boundary layer, surface-tension effects are important and capillary suction will act to drain liquid from the bulk fiber into the droplet.[19] Consequently, the resulting fiber will be approximately uniform along its entire length following drawing. Due to the uniform nature of the fiber shape during the drawing stage before fracture, the fiber will also continue to thin uniformly during the evaporation stage. As a result, both the drawing and evaporation stages ensure that uniform fibers are generated, which rationalizes the observations in Figure 1e (and other spinning processes). The inclusion of polymers in a fluid has also been shown to facilitate the fabrication of cylindrical fibers, corroborating this observation.[20]

In Figure 2a, the fiber diameter is observed to increase with PEO concentration, which we identify with an increase in viscosity. This result may be attributed to the fact that a viscosity increase raises the axial viscous stresses, which impede the stretching. The solution to the system (1)–(2) confirms this observation, predicting an increase in fiber diameter with increasing capillary number (Figure 2d). This analysis also highlights the importance of evaporation, with no dependence of fiber diameter on capillary number exhibited in the absence of evaporation (Figure 2d).

We have also demonstrated the simplicity and scalability of this new touch-spinning method by using a round hairbrush composed of the order of 600 filaments (**Figure 3**a). The brush was attached to an electrical motor via the brush grip. The setup was fed by a PEO solution poured onto a Teflon film placed underneath the round brush so that the brush filaments touched the droplets of the polymer solution but did not scratch the film. In Figure 3a, PEO solution is mixed with a dye for visualization purposes. Nanofibers were brush-spun from the free-liquid surface with a rotating hairbrush. Figure 3b,c shows the 200 nm nanofibers produced in 1 and 5 min, respectively, at 3000 rpm, and an SEM image of the resulting fibers is shown in Figure 3d. The total length of the fibers produced by the 600-filament brush with $D_s = 60$ mm at 3000 rpm in 5 min is 1700 km, which is a sufficient amount for a typical tissue-engineering experiment.

Depending on the rotational mode of the spinning frame, the touch-spinning process enables both regular and random fiber meshes and continuous single free-standing nano- and microfibers. For example, a rotating stage with a diameter of 5 cm was used to produce single free-standing 15 cm-long polyacrylonitrile (PAN) microfibers and PCL nanofibers. Deviation of the fiber diameter along their length and between different batches is in the range 3%–5%. The Young's modulus of PCL fibers with diameters from 650 to 800 nm was measured to be 0.26 ± 0.08 GPa, using a three-point bending test and an atomic force microscope (detailed procedure described in the Supporting Information). Such results are comparable

Adv. Mater. **2015**,
DOI: 10.1002/adma.201502768

with the mechanical properties of PCL fibers produced by other common methods.[21]

The essential difference of the touch-spinning method from other commonly used methods of nanofiber fabrication is in the mechanical control and manipulation of nanofibers that it offers. In contrast to all other methods, in touch-spinning, single filament nanofibers are drawn by the mechanical force that not only determines fiber stretching but also guides fibers onto the spool, providing better control over fiber alignment. For example, considering applications of nanofibers for tissue engineering scaffolds,[10] touch-spinning offers a very fast and practical method to produce scaffolds for cells with controlled mesh size in virtually any laboratory facility with no special requirement for equipment and training of personnel. For example, a supporting frame 15 mm × 15 mm size was placed behind the touch-spinning needle and fibers were collected on the frame (**Figure 4**a,b). After 2 min, the frame was rotated by 90° and touch-spinning was continued for 2 min more,

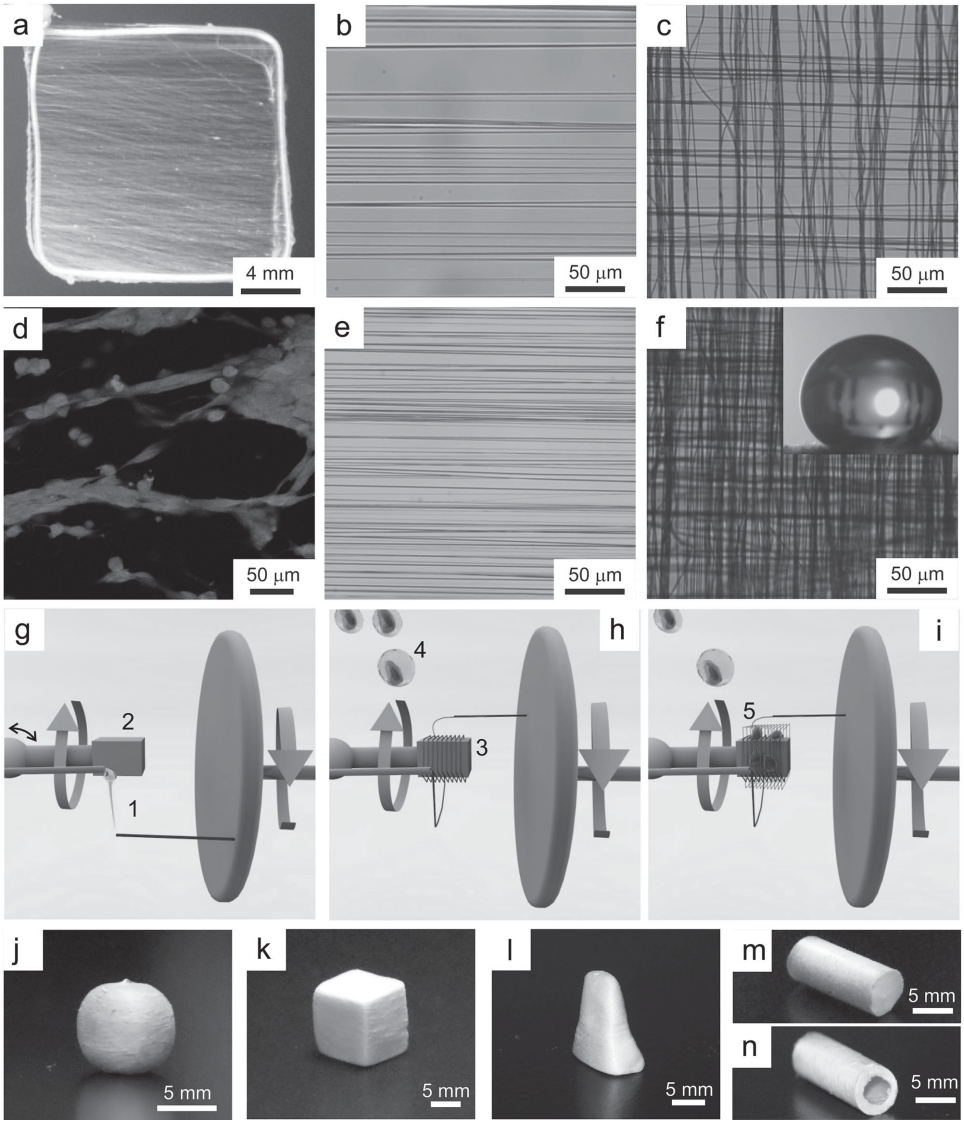

Figure 4. Nanofiber meshes with controlled mesh size for tissue-engineering and filtration applications. a) A 15 mm × 15 mm metallic frame size is placed behind the touch-spinning needle and fibers are collected on the frame. b) Optical microscopy image of fibers on the frame produced after 2 min of touch-spinning. c) After 2 min, the frame was rotated by 90° and touch-spinning was continued for 2 min more, resulting in a 28 ± 7 μm square mesh. d) Confocal image of the mouse breast cancer cell grown on the mesh. e) Optical microscopy image of fibers on the frame produced after 4 min of touch-spinning. f) After 4 min, the frame was rotated by 90° and touch-spinning was continued for 2 min more, resulting in a 5.8 ± 1 μm size mesh. Inset shows water droplet on the mesh of teflon nanofibers (contact angle = 154°). g–i) Preparation of 3D scaffolds by touch-spinning and simultaneous spraying of cells: g) The fiber drawn by the rod (1) is wound onto the frame (2) of a desired shape (a cuboid for example) attached to the spool. The spool can be tilted at any angle to wind fibers onto frames with complicated geometries. h) Fibers are wound onto the frame with a controlled density (3) that can be regulated by the motion of the spool that shuttles back and forward. NIH-3T3 mouse fibroblast cells (4) are sprayed onto the frame simultaneously with winding of fibers. i) 3D scaffold is made of the highly cellularized fiber meshes (5). j–n) Different shapes and sizes of 3D scaffolds obtained by winding nanofibers onto supporting frames mounted on a spool.

resulting in a 28 ± 7 µm square mesh (Figure 4c). The mesh size can be controlled by adjusting the time of touch-spinning: 4 min of touch-spinning produced a mesh with size 5.8 ± 1 µm (Figure 4e,f). The PCL meshes were successfully tested for scaffolding mouse breast cancer cells (Figure 4d). Owing to its very simple setup (Figure 4g–i), the highly cellularized wet 3D-scaffolds (Figure S6, Supporting Information) can be fabricated by combining fiber winding with simultaneous spraying of cells.[22] The examples illustrated in Figure 4j–n demonstrate the capability of the touch-spinning method for fabrication of biomimetic scaffolds on different scales from macroscopic shape and dimensions to microscopic fiber dimensions and alignment into various meshes that are relevant to mesh-like structures in human tissues.

Applications of the method developed are obviously not limited to tissue engineering scaffolds and extend to any other nanofiber application, for example filtration[23] when fibrous filters with a demanded mesh size can be prepared by simple winding of nanofibers as shown in Figure 4a–c. Another obvious example is the fabrication of fibrous superhydrophobic coatings.[24] Here, Teflon nanofiber meshes were tested for the fabrication of superhydrophobic surfaces (inset in Figure 4f).

In this report, we describe a new method for drawing nanofibers. The method is based on a very simple and inexpensive setup that does not require special training or skills. Using this method, nanofibers can be drawn in any non-specialized laboratory. It is possible to build a touch-spinning setup by gluing a surface-modified glass rod to a rotating stage from which fibers can be spun from a free-liquid surface. A simple hairbrush can be used to scale up the fiber drawing to spin kilometers of nanofibers per minute. Owing to the setup's simplicity and ability to manipulate nanofibers, 2D and 3D customized scaffolds of different dimensions, shapes, mesh sizes, fiber alignments, and combinations with biological materials can be easily fabricated in minutes.

Experimental Section

Polymer Solution Preparation: PCL (M_n = 80 000 g mol^{-1}) (Aldrich) was dissolved in chloroform (ACS grade, BDH, VWR) for 1 h at 60 °C to produce solutions with concentrations of 4 and 7 wt%. PEO (M_w = 400 000 g mol^{-1}) (Aldrich) was dissolved in deionized water for 4 h at 60 °C to produce 3.5, 5, 7, and 9 wt% solutions. PAN (M_n = 150 000 g mol^{-1}) (Pfaltz and Bauer, Inc.) was dissolved in *N*,*N*-dimethylformamide (DMF) (99.8%, extra dry, ACROS Organics) for 12 h at 60 °C to produce 8, 10, 12, and 14 wt% polymer solutions.

Surface Modification of the Glass Rod (*Preparation of Superhydrophobic Surface*): The glass rods (glass fibers) were cleaned in 1:1 ammonium hydroxide (50% v/v, VWR)/hydrogen peroxide (30%, Ward's Science) for 40 min. Following this, they were rinsed with deionized water. The glass rods were immersed for 15 h in 2% PFSTEOS (97%, Matrix Scientific) in toluene and then rinsed with toluene and ethanol (200 proof, KOPTEC) to remove any excess fluorosilane.

Preparation of Superomniphobic Surface: Superomniphobic surfaces were obtained by spraying of 8 wt% aqueous solution of silicon-carbide microrods. The average diameter and length of rods are 600 nm and 7 µm, respectively. The formation of silicon carbide rod aggregates was achieved in specially adjusted spraying conditions (Figure S3, Supporting Information). Deposition of these aerosol-assisted self-assembled structures led to production of re-entrant two-length-scale surface textures that help to stabilize the nonwetting regime. Following the deposition, the surface was functionalized with perfluorooctyltriethoxysilane.

Cell Culture: The mouse 4T1 breast tumor cells used for the present cultures were provided by Dr. Jin Xie, University of Georgia, USA. The growth medium consisted of Dulbecco's modified Eagle's medium (DMEM) containing 10% (v/v) fetal bovine serum with antibiotics. Cell cultures were maintained in a 37 °C incubator in a humidified atmosphere containing 5% CO_2. The cells were passaged at confluence using a standard trypsin protocol. The scaffolds made of PCL nanofibers were sterilized by UV light for 30 min. The nanofibers were then subjected to a rough collagen coating by immersing the nanofibrous scaffolds into a solution of calf skin collagen (0.1% solution in 0.1 M acetic acid) overnight. Afterward, the constructs were washed three times with PBS and kept air-dried. The 4T1 cells were seeded (1×10^5 cells cm^{-2}) and cultured on the collagen-coated fibers in Petri-dish culture plates for 2 days. Cell seeded scaffolds were then rinsed in phosphate-buffered saline, fixed in 3.7% formaldehyde solution and permeabilized with 1% (w/v) Bovine serum albumin prior to incubation with fluorescein-tagged phalloidin (Life Technology, NY, USA) at 0.1 mg mL^{-1} for 30 min. The cells were visualized using the 488 nm laser of a Zeiss LSM 710 inverted confocal microscope with a ZSMmeta head (Welwyn Garden City, UK). The images were analyzed using Image Pro Plus.

The mouse NIH-3T3 fibroblast cells used for the present cultures were purchased from ATCC, USA. DMEM containing 10% (v/v) fetal bovine serum with antibiotics was used for cell growth. Cell cultures were maintained in a 37 °C incubator in a humidified atmosphere containing 5% CO_2. Cells were passaged at confluence using a standard trypsin protocol. Cells were washed twice and stored in PBS buffer.

Supporting Information

Supporting Information is available from the Wiley Online Library or from the author.

Acknowledgements

This work was supported by funds of the University of Georgia. I.M.G. gratefully acknowledges support from the Royal Society through a University Research Fellowship. The authors thank Celeste Nelson for a helpful conversation.

Received: June 9, 2015
Revised: July 25, 2015
Published online:

[1] a) J. R. Venugopal, S. Low, A. T. Choon, A. B. Kumar, S. Ramakrishna, *Artif. Organs* **2008**, *32*, 388; b) S. Liao, B. Li, Z. Ma, H. Wei, C. Chan, S. Ramakrishna, *Biomed. Mater.* **2006**, *1*, R45.
[2] K. Ghanbari, S. Bathaie, M. Mousavi, *Biosens. Bioelectron.* **2008**, *23*, 1825.
[3] a) T. Tamura, H. Kawakami, *Nano Lett.* **2010**, *10*, 1324; b) S. Chen, H. Hou, F. Harnisch, S. A. Patil, A. A. Carmona-Martinez, S. Agarwal, Y. Zhang, S. Sinha-Ray, A. L. Yarin, A. Greiner, *Energ. Environ. Sci.* **2011**, *4*, 1417.
[4] a) A. Tokarev, O. Trotsenko, I. M. Griffiths, H. A. Stone, S. Minko, *Adv. Mater.* **2015**, *27*, 3560; b) Z.-M. Huang, Y.-Z. Zhang, M. Kotaki, S. Ramakrishna, *Compos. Sci. Technol.* **2003**, *63*, 2223.
[5] J. Huang, R. B. Kaner, *Nat. Mater.* **2004**, *3*, 783.
[6] a) S. Ramakrishna, K. Fujihara, W.-E. Teo, T. Yong, Z. Ma, R. Ramaseshan, *Mater. Today* **2006**, *9*, 40; b) P. Gibson, H. Schreuder-Gibson, D. Rivin, *Colloid. Surf. A* **2001**, *187*, 469; c) K. Graham, M. Ouyang, T. Raether, T. Grafe, B. McDonald,

P. Knauf, in *Fifteenth Annual Technical Conf. and Expo of the American Filtration and Separations Society*, AFS, Galveston, TX, USA **2002**, pp. 9–12.
[7] D. Li, J. Huang, R. B. Kaner, *Acc. Chem. Res.* **2008**, *42*, 135.
[8] a) D. Li, Y. Xia, *Adv. Mater.* **2004**, *16*, 1151; b) J. Doshi, D. H. Reneker, in *Conference Record of the 1993 IEEE Industry Applications Society Annual Meeting*, IEEE, Toronto, Canada, **1993**, pp. 1698–1703.
[9] M. R. Williamson, R. Black, C. Kielty, *Biomaterials* **2006**, *27*, 3608.
[10] a) H. Yoshimoto, Y. Shin, H. Terai, J. Vacanti, *Biomaterials* **2003**, *24*, 2077; b) M. Shin, H. Yoshimoto, J. P. Vacanti, *Tissue Eng.* **2004**, *10*, 33.
[11] a) W. L. Grayson, P. H. G. Chao, D. Marolt, D. L. Kaplan, G. Vunjak-Novakovic, *Trends Biotechnol.* **2008**, *26*, 181; b) V. L. Tsang, S. N. Bhatia, *Adv. Drug Deliv. Rev.* **2004**, *56*, 1635.
[12] a) T. Ondarcuhu, C. Joachim, *Europhys. Lett.* **1998**, *42*, 215; b) C. Joachim, *Europhys. Lett.* **1998**, *42*, 215.
[13] A. S. Nain, J. C. Wong, C. Amon, M. Sitti, *Appl. Phys. Lett.* **2006**, *89*, 183105.
[14] A. K. Kota, G. Kwon, A. Tuteja, *NPG Asia Mater.* **2014**, *6*, e109.
[15] a) P. Muthiah, S.-H. Hsu, W. Sigmund, *Langmuir* **2010**, *26*, 12483; b) R. Scheffler, N. S. Bell, W. Sigmund, *J. Mater. Res.* **2010**, *25*, 1595.
[16] a) X. Wang, T. Lin, *Needleless Electrospinning of Nanofibers: Technology and Applications*, PSP Ltd., Singapore, **2013**; b) M. R. Badrossamay, H. A. McIlwee, J. A. Goss, K. K. Parker, *Nano Lett.* **2010**, *10*, 2257.
[17] a) T. Hagen, *J. Applied Math. Mech.* **2002**, *82*, 545; b) F. T. Trouton, *Proc. R. Soc. London. A* **1906**, *19*, 426.
[18] R. Sattler, C. Wagner, J. Eggers, *Phys. Rev. Lett.* **2008**, *100*, 164502.
[19] C. Breward, P. Howell, *J. Fluid Mech.* **2002**, *458*, 379.
[20] a) A. Bazilevskii, S. Voronkov, V. Entov, A. Rozhkov, *Sov. Phys. Dok.* **1981**, *26*, 333; b) C. Wagner, Y. Amarouchene, D. Bonn, J. Eggers, *Phys. Rev. Lett.* **2005**, *95*, 164504; c) C. Clasen, J. Eggers, M. A. Fontelos, J. Li, G. H. McKinley, *J. Fluid Mech.* **2006**, *556*, 283.
[21] L. Sun, R. P. Han, J. Wang, C. Lim, *Nanotechnology* **2008**, *19*, 455706.
[22] J. J. Stankus, J. J. Guan, K. Fujimoto, W. R. Wagner, *Biomaterials* **2006**, *27*, 735.
[23] X. H. Qin, S. Y. Wang, *J. Appl. Polym. Sci.* **2006**, *102*, 1285.
[24] A. Tuteja, W. Choi, M. Ma, J. M. Mabry, S. A. Mazzella, G. C. Rutledge, G. H. McKinley, R. E. Cohen, *Science* **2007**, *318*, 1618.